ACS APPLIED MATERIALS & INTERFACES

Research Article

www.acsami.org

Method to Impart Electro- and Biofunctionality to Neural Scaffolds Using Graphene–Polyelectrolyte Multilayers

Kun Zhou,[†,‡] George A. Thouas,[§] Claude C. Bernard,[‡] David R. Nisbet,[⊥] David I. Finkelstein,[#] Dan Li,[†] and John S. Forsythe*[,†]

[†]Department of Materials Engineering and Monash Vision Group, and [‡]Monash Immunology and Stem Cell Laboratories, Monash University, VIC 3800, Australia

[§]Department of Zoology and [#]The Mental Health Research Institute, The University of Melbourne, VIC 3010, Australia

[⊥]ANU College of Engineering and Computer Science, Research School of Engineering, The Australian National University, ACT 0200, Australia

ABSTRACT: Electroactive scaffolds that are passively conductive and able to transmit applied electrical stimuli are of increasing importance for neural tissue engineering. Here, we report a process of rendering both 2D and 3D polymer scaffolds electrically conducting, while also enhancing neuron attachment. Graphene-heparin/poly-L-lysine polyelectrolytes were assembled via layer-by-layer (LbL) deposition onto 2D surfaces and 3D electrospun nanofibers. The employed LbL coating technique in this work enables the electro- and biofunctionalization of complex 3D scaffold structures. LbL assembly was characterized by a steady mass increase during the in situ deposition process in 2D, with regular step changes in hydrophobicity. Uniform coverage of the graphene/polyelectrolyte coatings was also achieved on nanofibers, with hydrodynamic flow and post-thermal annealing playing an important role in controlling sheet resistance of 2D surfaces and nanofibers. Cell culture experiments showed that both 2D and 3D graphene–PEMs supported neuron cell adhesion and neurite outgrowth, with no appreciable cell death. This electroactive scaffold modification may therefore assist in neuronal regeneration, for creating functional and biocompatible polymer scaffolds for electrical entrainment or biosensing applications.

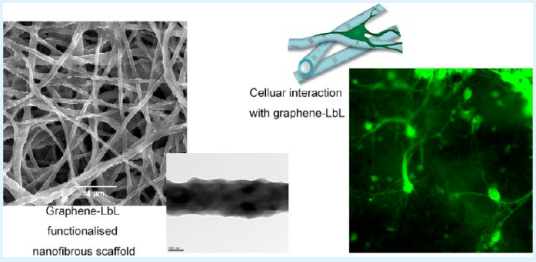

KEYWORDS: *layer-by-layer, graphene, polyelectrolyte multilayers, nanofibers, scaffolds, neural tissue engineering*

INTRODUCTION

Many important physiological functions involve electrical or charge transfer, especially at cell membrane interfaces. This process can be mediated actively using an applied current, i.e., to stimulate neurons[1,2] or muscle cells.[3] Recent research has also shown that cellular responses such as cell adhesion, proliferation, differentiation and signaling can be influenced by the passive conductivity of a substrate.[2,4] The ability to render biointerfaces electrically conductive opens the possibility of influencing cellular behavior, which also has potential benefits for therapeutic applications, such as tissue entrainment or physiological sensing. These characteristics can be achieved by utilization of charge conducting polymers[5] and carbon based materials which include carbon nanotubes (CNTs),[2,6] graphite[7,8] and graphene.[9,10] Among these conductive materials, graphene, the 2D carbon lattice, has shown novel and superior electrical, chemical and thermal properties in many research areas.[11,12] The high mobility of charge carriers,[12] intrinsic low electrical noise,[13] and reduced cytotoxicity when compared to CNTs[4,14] have made graphene a very viable candidate for tissue engineering and prosthetics.

Electronically conductive surfaces based on CNTs and graphene have been investigated widely. However, generally their manufacture involves complex procedures such as vapor deposition,[10] electrochemical deposition[15] or electrospraying,[6] which are expensive and have technical limitations such as high processing temperatures. In many cases, metal substrates and film transfer to other substrates is also required.[10] Self-assembly, a solution based coating strategy, provides a better approach to obtain nanometer thin films with less restriction on substrate chemistry, and is suitable for both 2D and 3D topographies. For surfaces based on graphene, covalent attachment is usually achieved by charged functional groups on its basal plane, followed by LbL assembly, as shown with oppositely charged species including metal nanoparticles,[16] chemically modified graphene[9] and polyelectrolytes.[17] However, the covalent attachment of charged functional groups is one of the main sources of increased electrical resistance due to disrupted electron conjugation.[18] Self-assembly of noncovalently modified graphene/polyelectrolyte substrates has also been achieved[13,19] on 2D substrates.

Here, graphene-LbL self-assembly was used to coat electrospun poly-ε-caprolactone (PCL) nanofibrous scaffolds, producing an electronically conductive 3D architecture with specific

Received: April 30, 2012
Accepted: July 18, 2012
Published: July 18, 2012

   dx.doi.org/10.1021/am3007565 | ACS Appl. Mater. Interfaces 2012, 4, 4524–4531

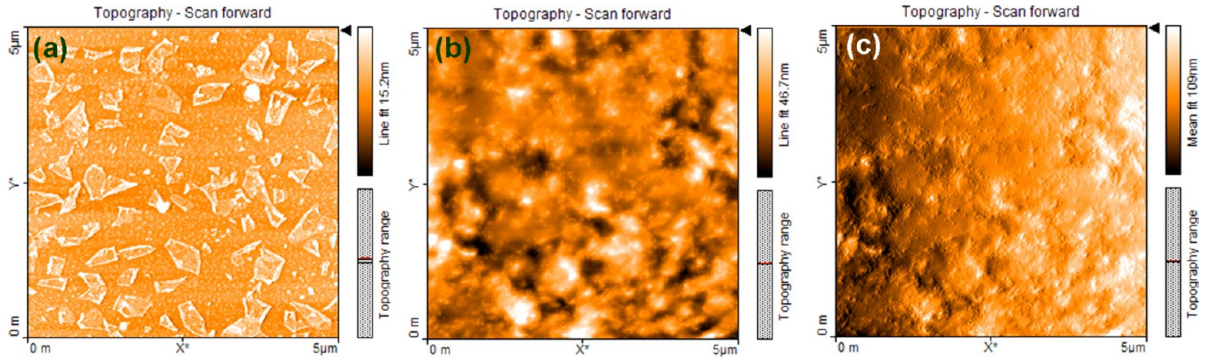

Figure 1. AFM color maps of 0.5 mg mL^{-1} graphene deposited on PEI-coated Si wafers, at (a) graphene−H1 layers and (b) graphene−P6. (c) A corresponding shaded map shows a 3D representation of b.

surface chemistry. In brief, aqueous colloidal suspensions of graphene nanosheets prepared from chemical reduction of exfoliated graphene oxide[20] were incorporated in a LbL assembly with nanoscale precision. The conductivity of the resulting graphene−PEMs composite arises from the 2D contacts between graphene sheets.[10] The 3D presentation of an electron conductive environment was achieved by combining electrospun nanofibers, characterized by their large surface to volume ratio and interconnected pores[21,22] and graphene−PEMs. Heparin, a highly negatively charged polysaccharide was employed to form nano layers of variable thickness in combination with poly-L-lysine (PLL), a cationic polypeptide with excellent cell adhesion properties.[23,24] In addition to the negative charged nature of heparin, more importantly, its potential anti-inflammatory, antiadhesive properties and specific binding to growth factors could provide approaches to reduce the inflammatory response and loading of growth factors.

Material characterization was performed on 2D and 3D substrates to assess the effects of graphene concentrations and hydrodynamic flow on self-assembly of graphene−PEMs. The functionality of the constructed PEMs was also assessed using sheet resistance measurement, and biocompatibility of LbL scaffolds were assessed for their ability to support in vitro culture of primary cortical neurons.

RESULTS AND DISCUSSION

Material Surface Characterization. The structural features of graphene−PEM surface morphology assembled on a 2D polyethyleneimine (PEI)-coated silicon wafer were studied using atomic force microscopy (AFM). Graphene nanosheets with an average size of 320 ± 120 nm, were distributed evenly on the 2D substrate after each LbL deposition (Figure 1a). The maximum average surface roughness was 17 nm for a 25 μm^2 area on 0.5 mg mL^{-1} graphene−P6 surface (the sixth graphene−PLL as the terminating layer, Figure 1b, c) compared to an average roughness of 1.6 nm for graphene-free H6 surfaces (the sixth heparin as the terminating layer). The graphene nanosheets were not visible using AFM following the PLL depositions, indicating they were buried beneath the PLL terminating layer (Figure 1b, c).

Mass deposition analysis using quartz crystal microbalance with dissipation (QCM-D) provided an important method to reference the LbL depositions on 3D PEI activated sample surfaces. Two different graphene concentrations (0.15 and 0.5 mg mL^{-1}) were incorporated with heparin (5 mg mL^{-1}) in PBS solution as the polyanion for deposition. As shown in Figure 2, the graphene-PEM deposition began with a very small change in $\Delta f/\nu$ for the first PLL and graphene−heparin depositions, at both graphene concentrations. A large frequency shift was then observed for both concentrations, beginning from the second graphene-heparin adsorption step. During the graphene-heparin adsorption, the magnitude of $\Delta f/\nu$ remained constant

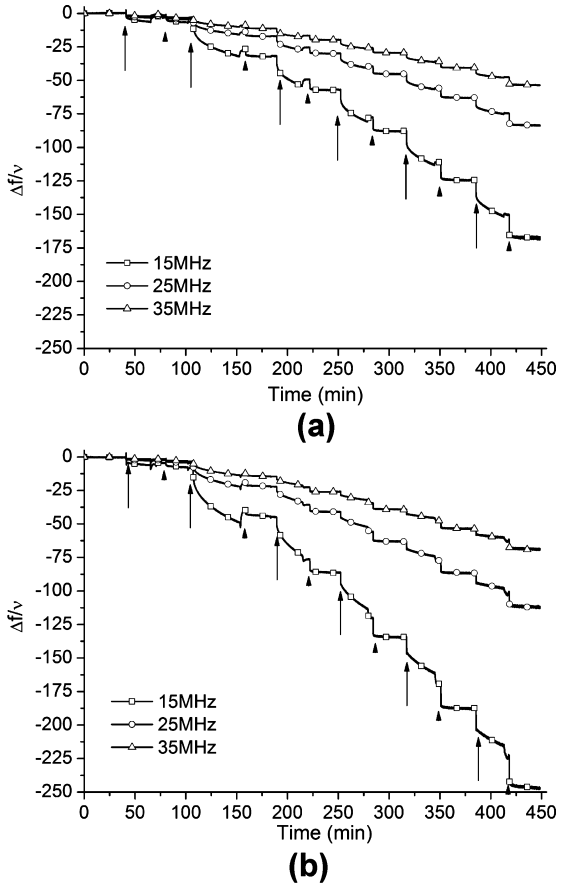

Figure 2. Assessment of mass deposition using QCM-D frequency shift ($\Delta f/\nu$) analysis of graphene−PEMs on PEI-coated QCM-D sensors with (a) 0.15 mg mL^{-1} graphene and (b) 0.5 mg mL^{-1} graphene in 5 mg mL^{-1} heparin/PBS as the respective polyanion. Black arrows showed the point of graphene−polyanion injection and arrowheads show the injection of PLL. PBS washes after each deposition step are not indicated. For clarity purposes, only every 6000 points from the collected data set were shown in these plots.

dx.doi.org/10.1021/am3007565 | ACS Appl. Mater. Interfaces 2012, 4, 4524−4531

for both (about 20 Hz for 0.15 mg $mL^{-1}$and 30 Hz for 0.5 mg mL^{-1} graphene respectively) at the third overtone during the entire LbL assembly cycle. Conversely, there was an increase in $\Delta f/\nu$ after each PLL injection during the assembly process in both groups. The 0.5 mg mL^{-1} graphene group exhibited a much larger change in $\Delta f/\nu$ (−247 Hz) compared to 0.15 mg mL^{-1} graphene group (−167 Hz) at the third overtone. As a first approximation, given that graphene nanosheets were found deposited evenly on the 2D surface prior to PLL deposition by AFM, the frequency changes were taken to be proportional to the mass adsorption. For the 0.5 mg mL^{-1} graphene group, a higher mass deposition on PEI coated QCM-D sensors was also observed. In the PBS wash step for the 0.15 mg mL^{-1} graphene group, there was an increase in the $\Delta f/\nu$, corresponding to the removal of loosely attached polymer. Interestingly, a decrease in $\Delta f/\nu$ for the 0.5 mg mL^{-1} graphene group was also observed, indicating that further mass adsorption occurred under hydrodynamic flow conditions. Collectively, these results confirm that regular mass deposition occurred after each self-assembly cycle for both graphene concentrations.

Following mass deposition analysis, the evolution of graphene-PEM surface chemistry on PEI activated 2D PCL surfaces was studied by contact angle (CA) measurement, which is sensitive to surface chemistry of the outermost 10−20 Å.[25] Alternating step changes in CA values were observed for both graphene and graphene free PEMs (Figure 3), indicating a

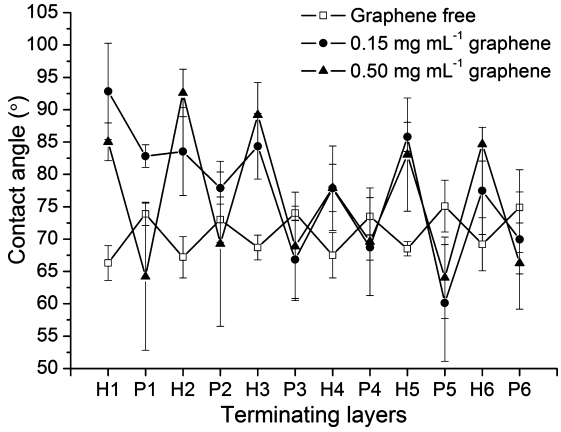

Figure 3. Contact angle values for heparin (H) and poly-L-lysine (P) terminating LbL surfaces using 0.15 mg mL^{-1} graphene (closed circle) and 0.5 mg mL^{-1} graphene (closed triangle), compared to graphene-free surfaces (open square). (Average of 3 readings for each point, error bars show standard deviations).

significant change in surface composition after each additional layer of polyelectrolyte or graphene-polyelectrolyte. However, an opposite pattern of the CA values was observed between graphene-free versus graphene-inclusive depositions, where the former PLL layers are more hydrophobic than heparin layers (74° compared to 68°), while the latter graphene-heparin layers showed much higher CA values than PLL layers even at a low graphene concentration of 0.15 mg mL^{-1} (about 85° compared to 68° for the last 3 bilayers). This can be explained by the hydrophobic nature of graphene nanosheets,[26] which influenced the surface energetics from beneath the PLL terminating layer. Notably, the increase in graphene concentration (from 0.15 to 0.5 mg mL^{-1}) did not increase the hydrophobicity of specific graphene-heparin layers.

Further information about the surface morphology of graphene-PEMs self-assembled on 3D PCL nanofibers was studied using electron microscopy. Since graphene nanosheets have an average size of 324 nm, as characterized by AFM analysis, they are able to diffuse through the micropores of the electrospun scaffolds to individual nanofiber surfaces. After building up graphene−P6−PEMs on PCL nanofibers, the fiber diameter increased from 310 ± 90 nm (n = 50) to 450 ± 140 nm (n = 50) (Figure 4a−c), with a relatively smooth surface of

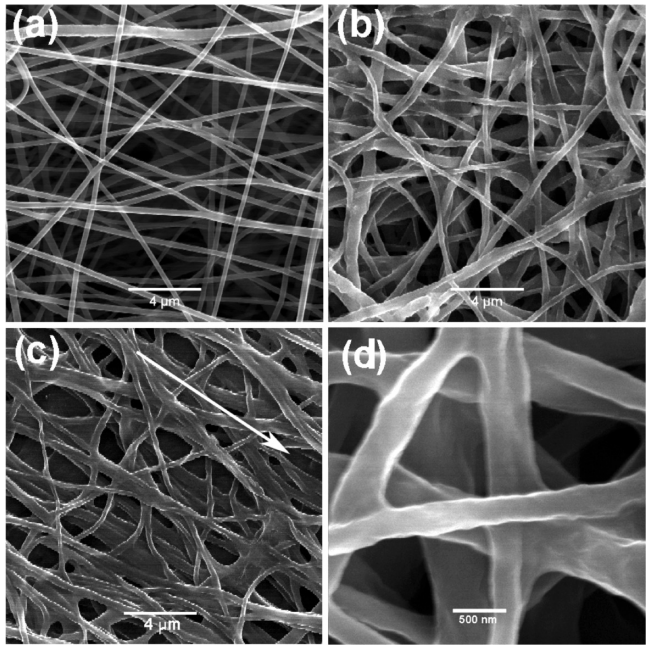

Figure 4. SEM images of (a) unmodified electrospun PCL nanofibers, graphene−P6 self-assembled on PEI activated PCL (b) random, (c) partially aligned nanofibers, and (d) high-magnification images graphene−P6 on nanofiber surfaces. All graphene−PEM samples were prepared under flow conditions. White arrow in c indicate the orientation direction of aligned fibers.

graphene-P6 as shown by scanning electron microscopy (SEM) (Figure 4d). Transmission electron microscopy (TEM) imaging of nanofibers showed a rough surface morphology initially (Figure 5c), which became smooth after successive layers, with the graphene-H4 layer being uniformly distributed (Figure 5b, c). A similar roughness was also initially observed in the graphene-free system, indicating that the surface roughness was not necessarily caused by the incorporation of graphene nanosheets into the polyelectrolytes. The mechanism for the formation of this surface roughness is not clear, but could possibly be due to the nanoscale curvature of the fiber surface influencing the arrangement of adsorbed polyelectrolyte polymer chains, since this rough surface was not observed on 2D substrates. However, it is important to note that the nanofibers were fully coated by graphene−PEMs or PEMs (Figure 5a) at the early deposition stage without any defects, even though the surface roughness was observed.

Electrical Conductance of Materials. The electrical properties of the graphene−PEMs functionalized on 2D and 3D PCL surfaces were studied in terms of sheet resistance measured by 4-point probe analysis. A progressive decrease in sheet resistance with increasing LbL assembly cycles of graphene-PEMs on the 2D surface was observed (Figure 6). For all the functionalized surfaces, sheet resistance showed a

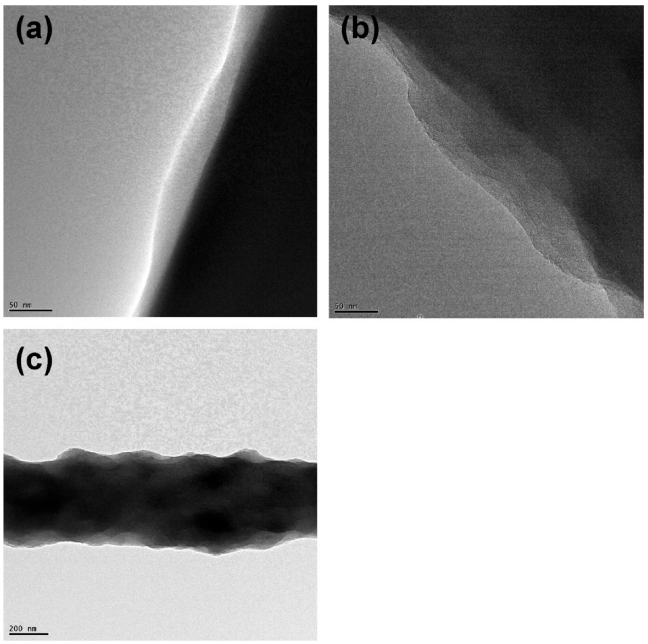

Figure 5. TEM images of (a) graphene-free H4 and (b) graphene−H4 functionalized nanofibers, with (c) graphene−H4 functionalized nanofibers at lower magnification, showing some degree of surface roughness, despite uniform coverage.

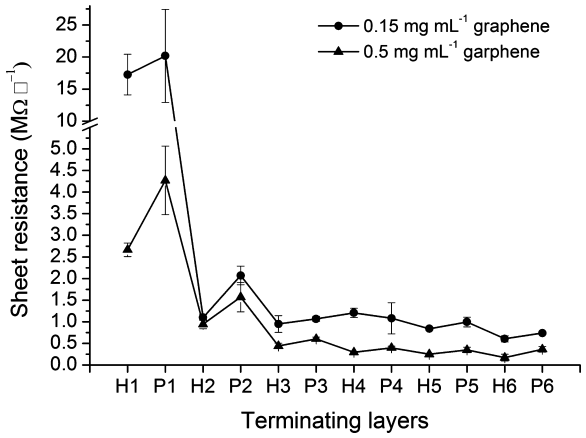

Figure 6. Sheet resistance of self-assembled graphene−PEMs of different terminating surfaces and layer number of heparin (H) or poly-L-lysine (P) (n = 4, error bars show the standard deviation).

concentration dependent trend, where lower sheet resistance was generally observed in the 0.5 mg mL^{-1} graphene group. Additional layers of PLL caused higher sheet resistance, which was especially evident for the initial 2 bilayers. Measured sheet resistance of the graphene-H1 surface suggests the formation of continuous contacts between graphene nanosheets over the PEI activated PCL surface. The sheet resistance difference (17.3 MΩ □$^{-1}$ and 2.67 MΩ □$^{-1}$) between 0.15 and 0.5 mg mL^{-1} graphene concentrations was directly proportional to the amount of graphene deposited, as shown by QCM-D (−2.97 Hz compared to −4.39 Hz at the third overtone). The graphene assembled during the graphene-H2 deposition step increased the surface coverage of graphene sheets, facilitating more contacts between individual graphene sheets, leading to a large drop in both the sheet resistance and $\Delta f/\nu$ values in the QCM-D. The small amount of PLL assembled during the first two PLL deposition steps ensured electrical percolation from the deposited graphene sheets from the previous and successive deposition steps. Due to the maximal graphene 2D contacts reached in the first five self-assembled cycles, as well as the increasing amount of deposited PLL, the values of sheet resistance stabilized and showed a small step change for every PLL or graphene-heparin layer. Though the following seven deposition layers did not contribute to a lower resistance, they are important to achieve a well structured and uniform coating for cellular interactions which we demonstrated in a previous study.[24] A sheet resistance of 0.74 and 0.36 MΩ □$^{-1}$ was observed for 0.15 and 0.5 mg mL^{-1} graphene groups, respectively, on graphene−P6 samples, confirming overall that graphene facilitated charge transfer across graphene−PEM surfaces in proportion to the amount used.

Graphene−P6-coated nanofibers prepared by quiescent adsorption during LbL deposition showed a consistently high resistance, which was beyond the measuring limit of the 4-point probe instrument. In relation to the QCM-D results, hydrodynamic flow further decreased the frequency change for the 0.5 mg mL^{-1} graphene group, indicating an effect of hydrodynamic flow on graphene-heparin deposition. The sheet resistance of graphene-PEMs self-assembled samples under flow conditions showed much lower values compared to those prepared under quiescent adsorption conditions (Table 1). For 2D samples, sheet resistance decreased from 362 to 24.6 kΩ □$^{-1}$; for the randomly orientated nanofibers, a sheet resistance of 203 kΩ □$^{-1}$ was recorded. The aligned nanofibers exhibited an anisotropic sheet resistance, where a sheet resistance of 408 and 109 kΩ □$^{-1}$ were found when measured perpendicular and parallel to the fiber orientation respectively. During the LbL deposition under flow conditions, heparin played a critical role in preventing graphene aggregation at the higher concentration (0.5 mg mL^{-1}). Considering the possible association between heparin chains via carboxylate/sulfate groups and graphene nanosheets,[27] the highly charged associated heparin chains may lead to the stabilization of the graphene solution (pure graphene aggregated after several deposition cycles). In addition, it was previously reported that hydrodynamic flow and electrostatic interactions resulted in higher deposition rates and required shorter times for polyelectrolytes to reach adsorption equilibrium.[28,29] We propose that the hydrodynamic flow also accelerates the deposition of graphene−heparin. Because the sheet resistance

Table 1. Average Sheet Resistance (kΩ □$^{-1}$) of Different Graphene−P6 Samples (0.5 mg mL^{-1})

sample groups	conventional soaking conditions	flow condition		postannealing at 60 °C for 24 h	
2D PCL	362	24.6		17.1	
random nanofibers		203		140	
aligned nanofibers	[a]	perpendicular	parallel	perpendicular	parallel
		408	109	240	86

[a]high resistance beyond the measuring limit of 4-point probe instrument.

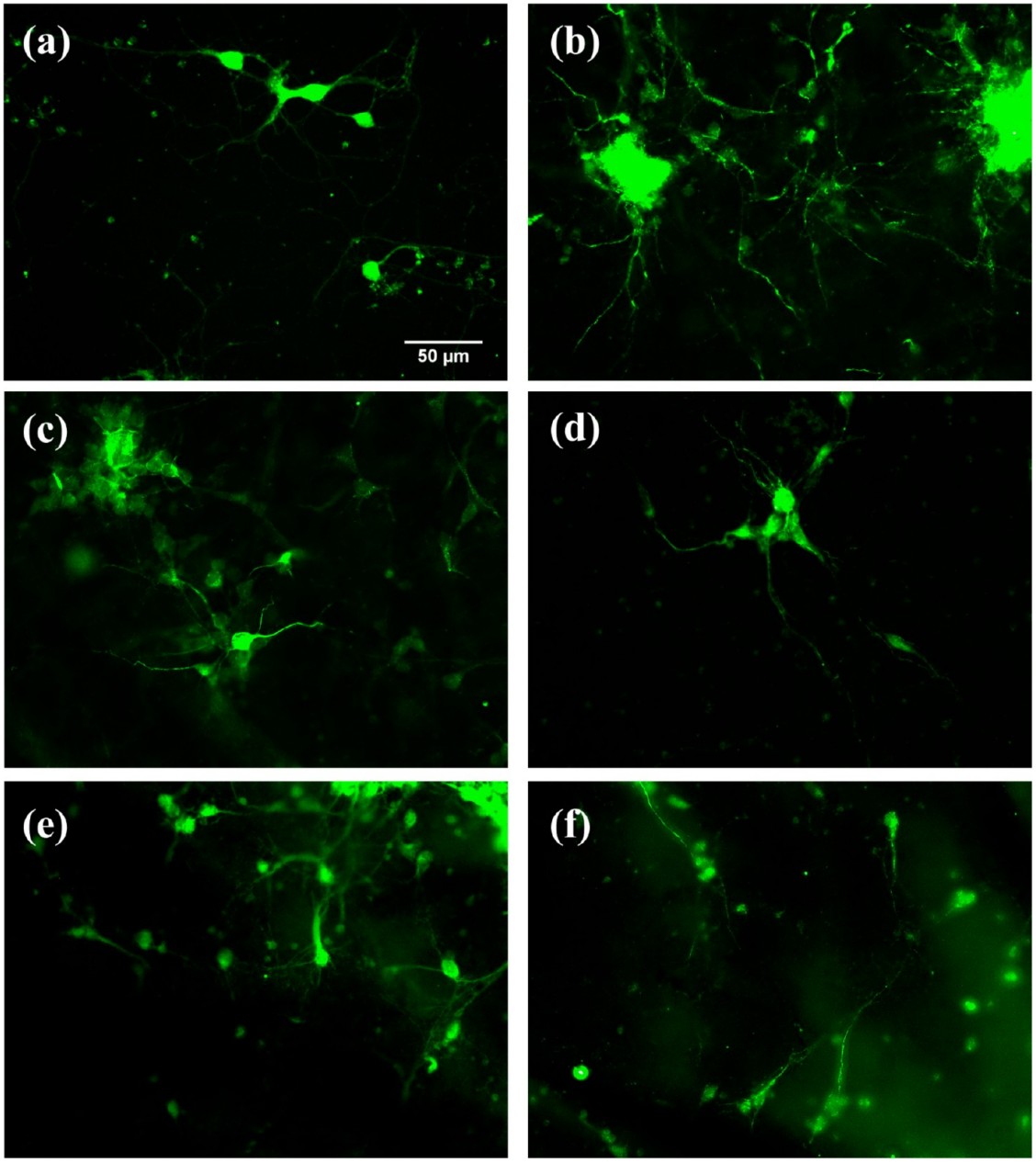

Figure 7. Fluorescence microscope images of Day 5 PCNs cultured on (a) PLL-coated glass coverslip (positive control); (b) unmodified PCL random nanofibers; (c) P6 random nanofibers; (d) graphene–P6 2D PCL substrate; (e, f) graphene–P6 random nanofibers. Neurons were stained with SMI-32 (green). All graphene–PEM-coated samples were prepared under flow conditions. Scale bar shows 50 μm for all images.

of graphene–PEMs was determined by the first four bilayers, the significant drop in resistance for samples prepared under flow conditions was possibly due to more graphene nanosheets deposited at each assembly step, and closer contacts between graphene sheets formed at earlier LbL depositions.

A further decrease in sheet resistance of the graphene–PEM coatings on 2D surfaces and 3D nanofibers was achieved by a post thermal annealing treatment (Table 1). After annealing graphene-P6 samples (prepared under flow conditions) at 60 °C for 24 h, the nanofiber morphology showed no difference to untreated controls (SEM images not shown). However the sheet resistance of graphene-P6 on 2D surfaces of the same nanofiber scaffolds decreased from 24.6 to 17.1 kΩ $\square^{-1}$ after annealing. Sheet resistance of the graphene-P6 on nanofibers also showed a decrease for the random nanofibers (203 to 140 kΩ $\square^{-1}$), and the aligned nanofibers (408 to 109 kΩ $\square^{-1}$ and 240 to 80 kΩ $\square^{-1}$, measured perpendicular and parallel to the fiber alignment, respectively). The further decrease in sheet resistance after heat treatment is possibly due to the densification of graphene-PEM structure,[30,31] which subsequently brings closer contact between adjacent graphene sheets within polyelectrolyte layers, and possibly between different layers of the PEM (especially for parallel aligned fibers, which might have more interfiber surface contacts than random fibers). This observation has also been reported for self-assembled CNT films after thermal treatment.[32]

Cell Culture on Materials. Cell morphology and neurite length of day 5 primary cortical neurons (PCNs) were assessed after 5 days of in vitro culture on 2D and 3D substrates, with the highest graphene concentration (0.5 mg mL^{-1}) assembled

under flow conditions. These were then compared to control groups, which were PLL-coated glass coverslips, graphene-free P6 coatings (positive controls) and unmodified PCL nanofibers. PCNs immunostained for SM1−32 protein, visualizing neuronal cell bodies, dendrites, axons, indicated no obvious morphology differences between groups (Figure 7b, c, e, f). Although PEM-free controls showed similar individual cell morphology to the PEM inclusive test groups, the number of attached cells on the unmodified PCL nanofiber surfaces was decreased, especially for the 2D surfaces (data not shown), which is in agreement with our previously reported observations of interactions of stem-cell-derived neurons.[24] Interestingly, cell clusters were observed only for cultures on unmodified PCL nanofibers (Figure 7b, bright green). This clustering of cells is indicative of poor cell−nanofibrous substrate interactions,[36,37] and indicates that the LbL coatings improved cell attachment and spreading on the nanofibers. Branched and elongated neurites were observed on graphene-P6 functionalized 2D and nanofibrous substrates (Figure 7d−f), showing similar morphology to PLL positive controls (Figure 7a) Following measurement of neurite length on unmodified PCL, graphene-free P6 and graphene−P6-modified nanofibers, the three groups showed average neurite lengths of 57 ± 4, 61 ± 6, and 74 ± 7 μm respectively (mean ± standard error of the mean). The similar level of neurite outgrowth on of the P6 and graphene−P6 nanofibers suggests that the inclusion of graphene nanosheets is not detrimental to the attachment and neurite extension of PCNs on PLL terminating layers, following LbL deposition.

■ CONCLUSIONS

The successful functionalization of 2D surfaces and 3D nanofibrous scaffolds complex structure was demonstrated, via the self-assembly of aqueous colloidal graphene. Uniform and controllable coverage of graphene-PEMs was observed on 2D surfaces and 3D nanofiber surfaces, with some nanoscale surface roughness that was alleviated with subsequent layers. The initial graphene concentration within the heparin solution together with the influence of hydrodynamic flow conditions during the first six deposition steps were critical manufacturing determinants of mass deposition and specific sheet resistance of 2D surfaces and 3D nanofibers. The addition of a thermal treatment after the graphene-PEM functionalization of both surface types further lowered sheet resistance (362 to 17.1 KΩ $\square^{-1}$ for 2D surfaces, 408 to 86 KΩ $\square^{-1}$ for nanofibers). Once functionalized, graphene-modified surfaces encouraged neurite outgrowth as the same level as poly-L-lysine alone, confirming that the presence of graphene in polyelectrolytes was not detrimental to the biocompatibility of the polyelectrolyte terminating layers. This work details the solution based graphene-LbL technique to electro- and biofunctionalize nano- to microscale scaffolds with complicated internal structures. The resulting 3D architecture with tunable electronic conductivity and specific surface chemistry can be designed to accommodate cell processes and whole cell bodies, potentially providing benefit in neural regeneration processes.

■ EXPERIMENTAL SECTION

Graphene Preparation. The graphene oxide synthesis process is described elsewhere.[20] In general, purified graphite oxide was dispersed in deionized water (2 mg mL^{-1}). Exfoliation of graphite oxide was performed by ultrasonication (750W, Sonics & Materials Inc., US) using a 50% amplitude, 30 min. Twenty mL of the ultrasonicated suspension was mixed with 175 μL ammonia solution (28 w/v%, Ajax Finechem, Australia), 200 μL hydrazine solution (35 wt % in water, Sigma-Aldrich) and deionized water to a final volume of 50 mL. The reduction process carried out at 95 °C in a water bath for 3 h.

2D and 3D Scaffold Preparation. 2D PCL (Sigma-Aldrich, St Louis, MO, USA, molecular weight =70000 − 90000) substrate was compression molded at 80 °C. 3D PCL nanofibrous scaffolds were prepared via electrospinning 11 w/v% PCL dissolved in 3:1 volume ratio of chloroform and methanol (MERCK Pty. Ltd. VIC, Australia) with 0.06 w/v% NaCl performed using an electrospinner 2.2.D-350 (Yflow Nanotechnology Solutions, Spain). A flow rate of 2 mL h^{-1}, a working distance of 10 cm and voltage of 11 kV was used. The collecting mandrel was adjusted to 500 or 800 rpm to achieve random and aligned nanofiber morphology. After the 50 min, scaffolds were collected and then dried overnight under vacuum.

Graphene LbL Deposition on 2D and 3D Scaffolds. All polyelectrolytes were dissolved in 0.25× PBS buffer (pH 7.4) for graphene LbL deposition. Two different graphene concentrations (0.15 and 0.5 mg mL^{-1}) were used. In brief, 2D PCL samples were washed with 80% ethanol/deionized water followed by ultrasonication for 30 s, rinsed with deionized water; 3D PCL nanofibers were wet with 80% ethanol/deionized water, thoroughly rinsed with deionized water. Both 2D and 3D scaffold surfaces were activated by soaking in 20 mg mL^{-1} polyethyleneimine (PEI, molecular weight = 750 000, Sigma-Aldrich, St Louis, MO, USA) in PBS buffer (pH 7.4) solution for 2 h rinsed in PBS. Scaffolds were then dipped into 5 mg mL^{-1} heparin (180USP units mg^{-1} Sigma-Aldrich, St Louis, MO,USA) with/without graphene for 25 min, followed by 15 min rinsing in PBS buffer, and then another 25 min soaking in 1 mg mL^{-1} PLL (molecular weight = 130 000 Sigma-Aldrich, St Louis, MO, USA). The deposition cycle was repeated and samples were collected. Assembly on the silicon wafer followed the same procedure. Samples prepared under flow conditions were conducted using the same conditions as above and were also stirred at a speed of 18 rpm in the polyelectrolyte solution. All graphene-PEMs samples were cross-linked with 2 w/v% N-(3-dimethylaminopropyl)-N′-ethylcarbodiimide hydrochloride (EDC) in PBS for 2 h, followed by thorough washing in deionized water.

4-Point Probe Resistance Measurements. Sheet resistance of graphene-PEMs modified 2D and 3D samples were measured by a previously reported technique using a 4-point probe (RM3-AR, Jandel Engineering Ltd., UK).[33−35] A constant current was applied through the conductive layers and the sheet resistance was recorded. For aligned nanofibers with electroactive coatings, the 4-point probe measurements were performed parallel and perpendicular to the fiber alignment direction.

Contact Angle Measurements. Hydrophilicity of the graphene-PEMs on 2D surfaces was determined by CA measurements, using the standard sessile drop technique on a video-based CA meter (Technical data OCA 20). Contact angles were measured on CCD camera images using SCA202 software (Dataphysics, Germany). Measurements were performed at 3 random locations on graphene−PEM or PEM surfaces, which had been predried overnight in a vacuum oven at room temperature.

Scanning Electron Microscopy. The morphology of graphene−PEMs and PEMs functionalized 3D scaffolds were characterized by scanning electron microscopy (SEM, JEOL JSM-6300F field emission). Prior to imaging, all samples were coated with 1 nm platinum. SEM images were taken under 30 kV voltage and 8 mm working distance.

Transmission Electron Microscopy. Graphene sheets embedded in PEMs were studied using TEM. PCL nanofibers were electrospun onto 300 mesh TEM gold grids (Agar Scientific Ltd., UK) for 10 s under the above electrospinning conditions. The TEM grids were then dipped into polyelectrolyte solutions for LbL deposition to obtain 4 bilayers of PEMs for better electron transmission. Vacuum-dried TEM grids were mounted onto the sample holder and then analyzed using a Phillips CM-20 TEM with a LaB6 filament at 200 kV. At these

settings, the point resolution was 0.27 nm. Images were acquired using a CCD camera (Gatan 831 SC600 Orius, 7 megapixels).

In vitro Culture of E14 Primary Cortical Neurons. All cell culture reagents used were purchased from Invitrogen, Mulgrave, Australia, unless specified below. Cortices were dissected from embryonic day 14 (E14) C57/B6 mice, followed by removal of meninges and olfactory bulbs (All the methods conform to the Australian National Health and Medical Research Council published code of practice for the use of animals in research and were approved by the Howard Florey Institute Animal Ethics Committee). Cortices were then treated with 0.025% trypsin in Krebs solution for 20 min at 37 °C. Dissociated primary cortical cells were resuspended in Dulbecco's modified Eagle's medium (DMEM, high glucose), supplemented with 10% fetal calf serum and 10 μg/mL gentamicin and then seeded onto sterilized scaffolds at a density of 0.15×10^6 cells cm^{-2}. After 2.5 h, the medium was removed and replaced by culture medium, which is composed of Neurobasal medium (NBM), supplemented with 0.5 mM glutamine, 2% B27 serum-free supplement and 10 $\mu g\ mL^{-1}$ gentamicin. Graphene−P6 on the 2D substrate and random/aligned nanofiber were used as test groups; graphene-free P6 on 2D substrate and random/aligned nanofiber were used as positive controls; unmodified PCL 2D and random/aligned nanofibers were used as negative controls. All cell culture samples were sterilized with 80% ethanol, and then allowed to air-dry in a laminar flow hood for 30 min. Sterile scaffolds were incubated in neurobasal medium for 2 h before seeding primary cortical neurones. Primary cortical neurones were cultured for 7 days at 37 °C with 5% CO_2 before immunostaining.

Immunocytochemistry. Cultured primary cortical cells were fixed with 4% paraformaldehyde for 10 min at room temperature, and then washed in PBS. Fixed cells were permeabilised in 0.2% Triton-X100 (Sigma-Aldrich, St Louis, MO, USA) for 5 min, followed by PBS wash. Nonspecific antibody binding was blocked with 3% normal goat serum (Vector Laboratories Ltd. UK) for 2 h at room temperature before PBS wash. Cells were then incubated in mouse-anti-SMI-32 neurofilament protein (1:500) in 1% BSA at 4 °C overnight. After subsequent washing in PBS, the cells were incubated in antimouse Alexa Flour 568 (1:800) at 37 °C for 1 h, followed by a PBS wash and DAPI nucleus staining (1:10,000) for 20 min.

Fluorescence Microscopy. Leica DFC310 FX fluorescence microscope equipped with a 40x numerical aperture of 1.25 was used to image the cells cultured on scaffolds. Images were obtained using Leica application suite (Leica, V3.3.0) software.

Neurite Measurements. PCNs cultured on unmodified PCL, P6 and graphene-P6 modified nanofibrous scaffolds were imaged using a fluorescence microscope. Neurite length in randomly chosen fields (n = 3) was measured using the ImageJ plugin − NeuronJ. Statistical analysis was performed using Mann−Whitney Rank Sum Test in GraphPad Instat software (GraphPad Software, Inc.)

AUTHOR INFORMATION

Corresponding Author

*E-mail: john.forsythe@monash.edu.

Notes

The authors declare no competing financial interest.

ACKNOWLEDGMENTS

This work was supported by ARC Special Initiative in bionic vision science & technology, ARC Discovery (DP0985433), the Contributing to Australian Scholarship and Science (CASS) Foundation, the Eva and Les Erdi AUSiMED Fellowship in Neurological Diseases, the Diana Asmar Fund, and the National Health and Medical Research Council of Australia.

REFERENCES

(1) Mazzatenta, A.; Giugliano, M.; Campidelli, S.; Gambazzi, L.; Businaro, L.; Markram, H.; Prato, M.; Ballerini, L. *J. Neurosci.* **2007**, *27*, 6931−6936.
(2) Cellot, G.; Cilia, E.; Cipollone, S.; Rancic, V.; Sucapane, A.; Giordani, S.; Gambazzi, L.; Markram, H.; Grandolfo, M.; Scaini, D.; Gelain, F.; Casalis, L.; Prato, M.; Giugliano, M.; Ballerini, L. *Nat. Nanotechnol.* **2009**, *4*, 126−133.
(3) Ebron, V. H.; Yang, Z.; Seyer, D. J.; Kozlov, M. E.; Oh, J.; Xie, H.; Razal, J.; Hall, L. J.; Ferraris, J. P.; MacDiarmid, A. G.; Baughman, R. H. *Science* **2006**, *311*, 1580−1583.
(4) Park, S. Y.; Park, J.; Sim, S. H.; Sung, M. G.; Kim, K. S.; Hong, B. H.; Hong, S. *Adv. Mater.* **2011**, *23*, H263−H267.
(5) Abidian, M. R.; Ludwig, K. A.; Marzullo, T. C.; Martin, D. C.; Kipke, D. R. *Adv. Mater.* **2009**, *21*, 3764−3770.
(6) Malarkey, E. B.; Fisher, K. A.; Bekyarova, E.; Liu, W.; Haddon, R. C.; Parpura, V. *Nano Lett.* **2008**, *9*, 264−268.
(7) Alazemi, M.; Dutta, I.; Wang, F.; Blunk, R. H.; Angelopoulos, A. P. *Adv. Funct. Mater.* **2009**, *19*, 1118−1129.
(8) Hendricks, T. R.; Lu, J.; Drzal, L. T.; Lee, I. *Adv. Mater.* **2008**, *20*, 2008−2012.
(9) Shen, J.; Hu, Y.; Li, C.; Qin, C.; Shi, M.; Ye, M. *Langmuir* **2009**, *25*, 6122−6128.
(10) Gunes, F.; Shin, H.-J.; Biswas, C.; Han, G. H.; Kim, E. S.; Chae, S. J.; Choi, J.-Y.; Lee, Y. H. *ACS Nano* **2010**, *4*, 4595−4600.
(11) Novoselov, K. S.; Geim, A. K.; Morozov, S. V.; Jiang, D.; Zhang, Y.; Dubonos, S. V.; Grigorieva, I. V.; Firsov, A. A. *Science* **2004**, *306*, 666−669.
(12) Bolotin, K. I.; Sikes, K. J.; Jiang, Z.; Klima, M.; Fudenberg, G.; Hone, J.; Kim, P.; Stormer, H. L. *Solid State Commun.* **2008**, *146*, 351−355.
(13) Zhang, B.; Cui, T. *Appl. Phys. Lett.* **2011**, *98*, 073116.
(14) Zhang, Y.; Ali, S. F.; Dervishi, E.; Xu, Y.; Li, Z.; Casciano, D.; Biris, A. S. *ACS Nano* **2010**, *4*, 3181−3186.
(15) Keefer, E. W.; Botterman, B. R.; Romero, M. I.; Rossi, A. F.; Gross, G. W. *Nat Nano* **2008**, *3*, 434−439.
(16) Zhu, C.; Guo, S.; Zhai, Y.; Dong, S. *Langmuir* **2010**, *26*, 7614−7618.
(17) Wang, D.; Wang, X. *Langmuir* **2011**, *27*, 2007−2013.
(18) Lomeda, J. R.; Doyle, C. D.; Kosynkin, D. V.; Hwang, W.-F.; Tour, J. M. *J. Am. Chem. Soc.* **2008**, *130*, 16201−16206.
(19) Liu, J.; Tao, L.; Yang, W.; Li, D.; Boyer, C.; Wuhrer, R.; Braet, F.; Davis, T. P. *Langmuir* **2010**, *26*, 10068−10075.
(20) Li, D.; Muller, M. B.; Gilje, S.; Kaner, R. B.; Wallace, G. G. *Nat Nano* **2008**, *3*, 101−105.
(21) Rnjak-Kovacina, J.; Weiss, A. S. *Tissue Eng., Part B: Rev.* **2011**, *17*, 365−372.
(22) Yang, F.; Murugan, R.; Wang, S.; Ramakrishna, S. *Biomaterials* **2005**, *26*, 2603−2610.
(23) Hu, M.; Sabelman, E. E.; Tsai, C.; Tan, J.; Hentz, R. V. *Tissue Eng.* **2000**, *6*, 585−593.
(24) Zhou, K.; Sun, G.; Bernard, C. C.; Thouas, G. A.; Nisbet, D. R.; Forsythe, J. S. *Biointerphases* **2011**, *6*, 189−199.
(25) Zisman, W. A., In *Contact Angle, Wettability and Adhesion: The Kendall Award Symposium Honoring William A. Zisman*; Los Angeles, April 2−3, 1963 ; Fowkes, F. M., Eds.; Advances in Chemistry Series; American Chemical Society: Washington, D.C., 1964; Vol. *43*.
(26) Wang, S.; Zhang, Y.; Abidi, N.; Cabrales, L. *Langmuir* **2009**, *25*, 11078−11081.
(27) Rai, B.; Grondahl, L.; Trau, M. *Langmuir* **2008**, *24*, 7744−7749.
(28) Nadezhda L, F. *J. Colloid Interface Sci.* **1999**, *211*, 336−354.
(29) Hoda, N.; Kumar, S. *J. Rheol.* **2007**, *51*, 799−820.
(30) Köhler, K.; Sukhorukov, G. B. *Adv. Funct. Mater.* **2007**, *17*, 2053−2061.
(31) Ibarz, G.; Dahne, L.; Donath, E.; Mohwald, H. *Chem. Mater.* **2002**, *14*, 4059−4062.
(32) Kam, N. W. S.; Jan, E.; Kotov, N. A. *Nano Lett.* **2008**, *9*, 273−278.

(33) Xuyen, N. T.; Ra, E. J.; Geng, H.-Z.; Kim, K. K.; An, K. H.; Lee, Y. H. *J. Phys. Chem. B* **2007**, *111*, 11350−11353.
(34) Gandhi, M.; Yang, H.; Shor, L.; Ko, F. *Polymer* **2009**, *50*, 1918−1924.
(35) Gilmore, K. J.; Moulton, S. E.; Wallace, G. G. *Carbon* **2007**, *45*, 402−410.
(36) Nisbet, D. R.; Pattanawong, S.; Ritchie, N. E.; Shen, W.; Finkelstein, D. I.; Horne, M. K.; Forsythe, J. S. *J. Neural. Eng.* **2007**, *4*, 35−41.
(37) Nisbet, D. R.; Pattanawong, S.; Nunan, J.; Shen, W.; Horne, M. K.; Finkelstein, D. I.; Forsythe, J. S. *J. Colloid Interface Sci.* **2006**, *299*, 647−655.